**Article ID:** 1000-324X(2022)03-0353-08 **DOI:** 10.15541/jim20210636

# Effect of Solid Loading on the Property of $Al_2O_3$ Ceramics in Stereolithographic Additive Manufacturing

LIU Guoqian[1], YAN Changhai[1], ZHANG Keqiang[2], JIN Hua[3], HE Rujie[2]

(1. Science and Technology on Space Physics Laboratory, China Academy of Launch Vehicle Technology, Beijing 100076, China; 2. Institute of Advanced Structure Technology, Beijing Institute of Technology, Beijing 100081, China; 3. School of Aerospace Engineering, Xiamen University, Xiamen, 361005, China)

**Abstract:** For ceramic stereolithographic (SL) additive manufacturing, the solid loading of ceramic photosensitive slurry plays an important role during the SL process. In this study, $Al_2O_3$ ceramics were fabricated by SL additive manufacturing from photosensitive $Al_2O_3$ slurries with various solid loadings, and the solid loading-property relationships of $Al_2O_3$ ceramic were performed. The effects of solid loading on not only the rheological behavior and curing property of the photosensitive $Al_2O_3$ slurry but also the microstructure and mechanical properties of the $Al_2O_3$ ceramic were investigated. The results showed that both the viscosity and shear stress increased with the increase of the solid loading. High viscosity was greater than the critical value for self-leveling during the SL process. The curing properties of photosensitive $Al_2O_3$ slurries were highly depended on the sold loading. Moreover, clear effects on the defect characteristics of $Al_2O_3$ ceramics manufactured from various photosensitive slurries were observed. These manufactured defects are critical for the mechanical behavior of $Al_2O_3$ ceramic. In addition, the relationship between rheological behavior and curing property of photosensitive $Al_2O_3$ slurry. Meanwhile, the resulting microstructure and mechanical properties of the $Al_2O_3$ ceramic were also illustrated. Inhomogeneous structure caused by high viscosity can lead to a sintered ceramic with poor strength. These findings provide fundamental understanding for SL additive manufacturing of ceramics.

**Key words:** $Al_2O_3$ ceramics; solid loading; stereolithography; additive manufacturing

Additive Manufacturing (AM) is a rapid prototyping technique based on the sequential layer-by-layer deposition, which provides possibility for the manufacturing of complex three-dimensional ceramic geometries with anisotropic macrostructure and/or microstructure, aiming to tailor structural or functional properties[1-3]. At present, several potential AM techniques have been reported[4-7]. Thanks to the high-quality parts with smoother surface and higher dimension precision, stereolithographic (SL) based on the UV polymerization of the photosensitive resin has received more attention[1,7-9]. For instance, due to its excellent chemical and mechanical properties, as well as thermal property, alumina ($Al_2O_3$) ceramic parts with complex shapes and working under high temperature and mechanically demanding environments have been manufactured using SL process[10-11].

During the SL process, $Al_2O_3$ ceramic green body was fabricated through layer-by-layer recoating of photosensitive slurry. To achieve a high efficient recoating, the slurry should have excellent fluidity and curing property. Usually, the viscosity of photosensitive $Al_2O_3$ slurry needs to be less than 3 Pa·s[12], which requires a moderate solid loading of the slurry. Li, *et al*.[13] have studied the rheological property of photosensitive $Al_2O_3$ slurry, and observed that the viscosity increased with the increasing of solid loading. Manufactured $Al_2O_3$ ceramic showed a high relative density of 95% from a slurry with a solid loading of 40% (in volume) and viscosity of 2.12 Pa·s. Many researchers tried various methods to obtain $Al_2O_3$ slurry with solid loading as high as possible, and viscosity as low as possible. Nie, *et al*.[14] added plasticizer to regulate the rheological behavior of photosensitive $Al_2O_3$ slurry used for SL, because the slurry with a high solid loading always exhibited a high

**Received date:** 2021-10-17; **Revised date:** 2021-11-09; **Published online:** 2021-12-24
**Foundation item:** National Natural Science Foundation of China (51772028)
**Biography:** LIU Guoqian (1980–), male, senior engineer. E-mail: 15201631565@163.com
刘国仟(1980–), 男, 高级工程师. E-mail: 15201631565@163.com
**Corresponding author:** HE Rujie, associate professor. E-mail: herujie@bit.edu.cn
何汝杰, 副教授. E-mail: herujie@bit.edu.cn

viscosity, causing defects and poor mechanical property of the final ceramic body. On the other hand, some researchers addressed the importance of the solid loading on the microstructure and mechanical property of the $Al_2O_3$ ceramic manufactured by SL. Azarmi, *et al.*[15] also manufactured $Al_2O_3$ ceramic from photosensitive slurry with a solid loading of 50% (in volume), and evaluated the microstructural features of the $Al_2O_3$ samples after printing, debinding and sintering process. The SL additive manufactured $Al_2O_3$ ceramic showed a porosity of approximately 8%, unfortunately, the mechanical property was not studied in depth. From previous studies, it is found that the solid loading plays a significant role in both the performance of photosensitive $Al_2O_3$ slurry and the microstructure and mechanical property of SL additive manufactured $Al_2O_3$ ceramic. In fact, the higher the solid loading is, the higher the viscosity is. A moderate solid loading is always required to manufacture parts with low defect, high densification and strength. Some works demonstrated that solid loading exhibited obvious effects on the microstructure and mechanical property of $Al_2O_3$ ceramic, however, previous works were limited to conventional techniques[16-17]. Thus only few works focused on the role of solid loading during SL additive manufacturing of $Al_2O_3$ ceramics, as well as the relationship between the rheological behavior of photosensitive $Al_2O_3$ slurry and the resulting microstructure and mechanical property of the $Al_2O_3$ sintered ceramic.

This study was attempt to provide a deep insight into solid loading-property relationships of $Al_2O_3$ ceramic manufactured using SL additive manufacturing. In this work, the influences of solid loading on the rheological behavior, curing property of the photosensitive $Al_2O_3$ slurry, and the microstructure, mechanical property of the $Al_2O_3$ ceramic were investigated and discussed. The relationship between the rheological behavior, curing property of photosensitive $Al_2O_3$ slurry and the resulting microstructure and mechanical property of the $Al_2O_3$ sintered ceramic were also illustrated.

# 1 Experimental

## 1.1 Starting materials

Two kinds of $Al_2O_3$ powders with different particle sizes were selected and mixed as raw powders. The weight ratio of fine grain $Al_2O_3$ (f-$Al_2O_3$, $d_{50}$=1.05 μm, Zhongzhou Alloy, China) and coarse grain $Al_2O_3$ (c-$Al_2O_3$, $d_{50}$= 10.34 μm, Zhongzhou Alloy, China) was 15 : 85. 3% (in mass) $TiO_2$ (rutile, 60 nm, Aladdin, China) and 1% (in mass) MgO (50 nm, Aladdin, China) based on as-mixed $Al_2O_3$ powders were added as sintering additives.

The as-mixed powders were dispersed in photosensitive resin and thinner, including TMPTA (Hengrong, China) and HDDA (Aladdin, China) with a volume ratio of 1 : 4. A small amount of TPO (1% (in mass) based on as-mixed photosensitive resin) was added as photoinitiator. In addition, to improve the fluidity of the photosensitive slurries, 2% (in mass) of KOS110 based on as-mixed $Al_2O_3$ powders was added as dispersant.

## 1.2 Slurry preparation

Firstly, starting materials were weighted and ball-milled by a planetary mill (Qmonoclinic3SP2, China) for 24 h at 400 r/min. Then, dispersed and stable photosensitive $Al_2O_3$ slurries with different solid loadings were obtained. In this study, the solid loading was set at 45%, 50%, 55%, 60% and 65% (in volume), respectively, named $S_{45}$, $S_{50}$, $S_{55}$, $S_{60}$, $S_{65}$.

## 1.3 SL additive manufacturing

An additive manufacturing equipment (10Dim, China) based on SL was subsequently applied to fabricate $Al_2O_3$ green bodies. Firstly, 3D model drawn by Solidworks software was sliced with a thickness of 50 μm. UV-light intensity and the exposure time were selected as 9000 $\mu W \cdot cm^{-2}$ and 4 s, respectively. Various $Al_2O_3$ green bodies, including rectangular bars (3.8 mm×5.0 mm×46 mm), cylinders ($\phi$25 mm×30 mm), were manufactured, respectively, as shown in Fig. 1. After manufacturing from the photosensitive slurries, $Al_2O_3$ green bodies were washed with ethanol to remove uncured slurry. Finally, $Al_2O_3$ ceramic green bodies were obtained.

## 1.4 Debinding and sintering process

$Al_2O_3$ green bodies were carefully heated for debinding, a heating rate of 0.5 ℃·$min^{-1}$ was adopted at the temperature range of 250–550 ℃ with a dwell time of 2 h, and then pre-sintering was conducted at 1000 ℃ for 2 h in a conventional muffle furnace (Facerom, China) in air. After that, the pre-sintered samples were subsequently transformed to another air furnace (Facerom, China) and sintered at 1600 ℃ for 2 h. Debinding and sintering procedures have been reported in detail in our

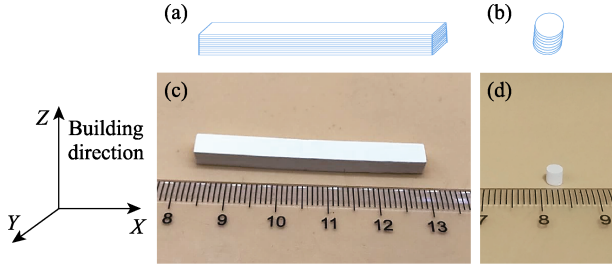


Fig. 1 (a, b) Schematic diagram of slicing model and (c, d) green bodies of rectangular bar and cylinder

previous work[18]. For simplicity, the as-sintered $Al_2O_3$ ceramics were denoted as A45, A50, A55, A60, and A65, respectively.

### 1.5 Characterization

Rheological behavior of the $Al_2O_3$ photosensitive slurries were tested using a rotational rheometer (Anton Parr., Austria) with a shear rate range of 0.01–200 $s^{-1}$ at 25 ℃. To evaluate the SL process, photosensitive $Al_2O_3$ slurries were exposed at various time (1–68 s) and the cured layer thickness was measured by a digital micrometer (Anyi, China).

The size of both green bodies and sintered samples were measured using a digital micrometer, and then the linear shrinkage can be calculated. The relative density of the $Al_2O_3$ ceramic was measured using Archimedes method. The flexural strength was tested using a three-point uniaxial bending test (Instron, USA). The loading span was 30 mm and the cross-head speed was 0.5 mm·$min^{-1}$ at room temperature. The standard, ISO-14704[19], was used as reference.

The fracture topography of the mechanical tested samples was observed using a scanning electron microscope (SEM, Zeiss, Germany). The internal defect features within the $Al_2O_3$ sintered ceramics were characterized by a X-Ray Computed-Tomography (X-CT, Zeiss, USA). An isotropic pixel size of 2.76 μm was obtained by binning two in each case.

## 2 Results

### 2.1 Rheological behavior of $Al_2O_3$ slurry

The effects of solid loading on the rheological behavior of these photosensitive $Al_2O_3$ slurries were performed firstly, as shown in Fig. 2. The viscosity *versus* shear rate for these photosensitive $Al_2O_3$ slurries was presented Fig. 2(a). The viscosity rises as the solid loading increasing. At the low solid loading of 45% and 50% (in volume), viscosity decreases with the increasing of shear rate and exhibits a typical shear thinning behavior. However, when the solid loading rises up to 55% (in volume), $Al_2O_3$ slurry shows a remarkable shear plateau behavior when the shear rate is lower than 100 $s^{-1}$, and then exhibits a slightly shear thickening behavior. However, when the solid loading is above 55% (in volume), $Al_2O_3$ slurry presents evidently shear thickening behavior.

As presented in Fig. 2(b), the relationship between shear stress and shear rate can be expressed by Hersche-Bulkley model[20]:

$$\tau = \tau_0 + K\gamma^n \tag{1}$$

where $\tau$ and $\tau_0$ refer to the shear stress and yield shear stress, respectively, $K$ refers to the consistency index, $\gamma$ is the shear rate, and $n$ is the flow behavior index. It should be noted that the difference between non-Newtonian fluid and Newtonian fluid is characterized by the degree of difference between $n$ and 1. The experimental data is fitted by Herschel-Bulkley Model, as presented in Fig. 2(b). And the fitted Herschel-Bulkley Model parameters are given in Table 1. The experimental values are in good agreement with the Herschel-Bulkley Model results, which is consistent with the $R^2$ result ($R^2$>0.998). At the low solid loading of 45% and 50% (in volume), the flow behavior index, $n$, is close to 1, indicating that the photosensitive $Al_2O_3$ slurry prepared from a low solid loading exhibits a near Newtonian fluid behavior. However, $n$ value increases as the solid loading increasing, demonstrating that the slurry exhibits a shear thickening behavior. Moreover, the yield shear stress of the photosensitive $Al_2O_3$ slurry increases from 1.24243 to 3.97074 Pa with the solid loading increasing from 45% to 65% (in volume), further revealing that the mutual attraction between $Al_2O_3$ particles increases with the increasing of solid loading.

To study the relationship between the rheological behavior and solid loading of photosensitive $Al_2O_3$ slurry in depth, the viscosities of photosensitive $Al_2O_3$ slurries with various solid loadings were studied at the shear rate of 200 $s^{-1}$, as shown in Fig. 2(c). When the solid loading is lower than 60% (in volume), the viscosity increases slowly which is lower than the critical viscosity value of

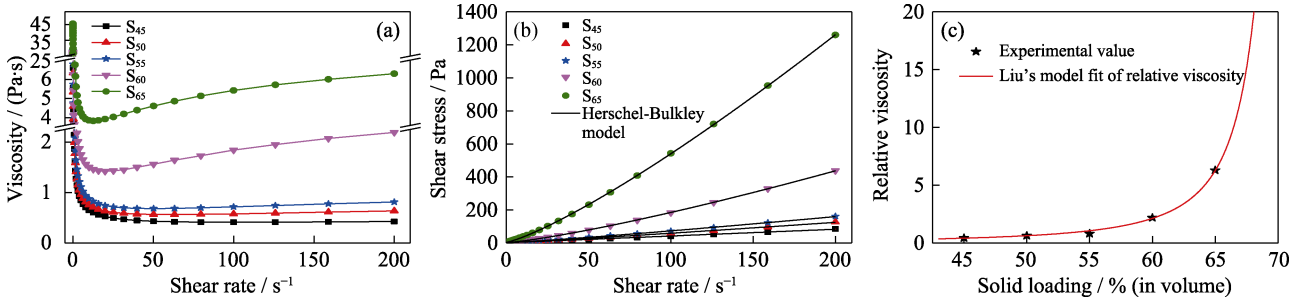


Fig. 2 (a) Apparent viscosity and (b) shear stress *vs* shear rate curves of photosensitive $Al_2O_3$ slurries with different solid loadings, and (c) relative viscosity dependence on solid loading at the shear rate of 200 $s^{-1}$

**Table 1 Herschel-Bulkley model parameters of $Al_2O_3$ slurries**

| Solid loading /% (in volume) | $\tau_0$/Pa | $K$ | $n$ | $R^2$ |
|---|---|---|---|---|
| 45 | 1.24243 | 0.41855 | 0.99596 | 0.99825 |
| 50 | 1.43614 | 0.37397 | 1.09476 | 0.99871 |
| 55 | 1.77148 | 0.37481 | 1.14081 | 0.99883 |
| 60 | 2.26134 | 0.57750 | 1.25022 | 0.99975 |
| 65 | 3.97074 | 1.87845 | 1.22798 | 0.99992 |

self-leveling (3 Pa·s) required for the SL process[12]. The viscosity then rises sharply as the solid loading increasing due to the severe agglomeration of the $Al_2O_3$ particles. At a higher solid loading, both Brownian motion and hydrodynamic interactions affect the rheological behavior[21]. Here, Liu's model[22] can be introduced to describe the relation:

$$\eta_r = [a(\phi_m - \phi)]^2 \quad (2)$$

where $\eta_r$ refers to the relative viscosity, $\phi$ and $\phi_m$ refer to the solid loading and maximum solid loading, respectively. The constant $a$ is determined experimentally. As given in Fig. 2(c), the $\eta_r$-$\phi$ plot is well fitted according to Eq. (2) ($R^2$=0.9972). Moreover, this model can predict the maximum particle packing density of a given powder, or maximum theoretical solid loading. In this regime, the constant is 0.057, and $\phi_m$ is 0.72, respectively, indicating that the maximum theoretical solid loading of the photosensitive $Al_2O_3$ slurry is around 72% (in volume) in this condition.

## 2.2 Curing property of $Al_2O_3$ slurry

In this study, UV-light intensity was set as 9 mW·cm$^{-2}$, the curing thickness *vs* exposure time of photosensitive $Al_2O_3$ slurry are shown in Fig. 3. With the exposure time increasing, the curing thickness increases at first and then trends to keep as a constant value. The curing thickness of the photosensitive $Al_2O_3$ slurry decreases as the solid loading increasing. During the curing process, UV-light is absorbed, scattered and reflected by $Al_2O_3$ particles. At the same time, the cured layer blocks the UV-light, which hinders the polymerization of the photosensitive resin and thereby affects the curing of the photosensitive $Al_2O_3$ slurry. Moreover, the higher the solid loading is, the less the curing thickness is. It is mainly because with the solid loading increasing, the UV-light absorbed by $Al_2O_3$ particles increases, correspondingly the UV-light absorbed by photosensitive resin decreases, which causes the curing thickness decreasing. In this study, the slicing thickness was set as 50 μm. To obtain a combination of interlayer and thus avoid delamination, curing thickness should be higher than the slicing thickness. In addition, long exposure time will lead to over-curing. Therefore, according to Fig. 3, the optimal exposure time must longer than 3 s and so be selected as 4 s.

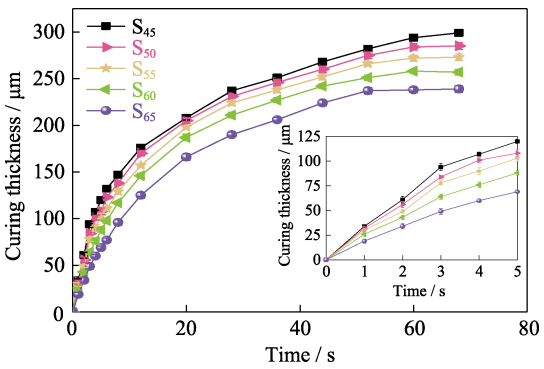


Fig. 3 Curing thickness *vs* exposure time of $Al_2O_3$ slurries with different solid loadings

## 2.3 Mechanical property and microstructure of $Al_2O_3$ ceramics

Fig. 4 shows the flexural strength and relative density of the $Al_2O_3$ sintered ceramics prepared from photosensitive slurries. It can be seen that the strength presents a strong dependence on the density of the sintered ceramic, which is consistent with the research of Ndinisa's result[16]. Moreover, both the strength and density increase firstly, the highest relative density of (94.46±0.41)% and flexural strength of (279.54±6.82) MPa are obtained from slurry with a solid loading of 50% (in volume), then the relative density and strength decrease with the increasing of solid loading. Interestingly, the strength obtained in this study is greater than some conventional methods. As mentioned above, the higher the solid loading is, the higher the viscosit is. It must be noted that high viscosity results in insufficient degassing and hinders the flow of photosensitive slurry, thereby air trapped and defects formed during the SL process. Hence, defects result in stress concentration in $Al_2O_3$ sintered ceramic and have a negative effect on the density and strength.

In addition, an inhomogeneous structure caused by high solid loading can also lead to sintered ceramic with

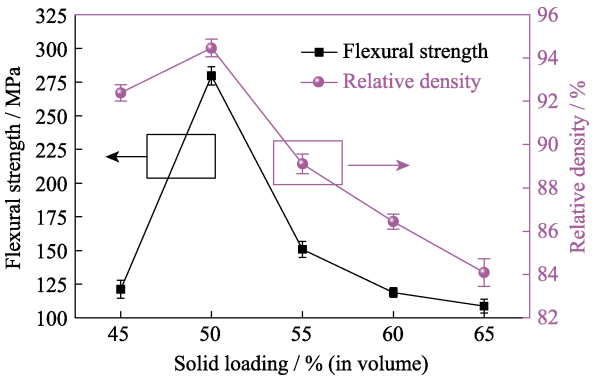


Fig. 4 Flexural strength and relative density of sintered $Al_2O_3$ ceramics varied with solid loading

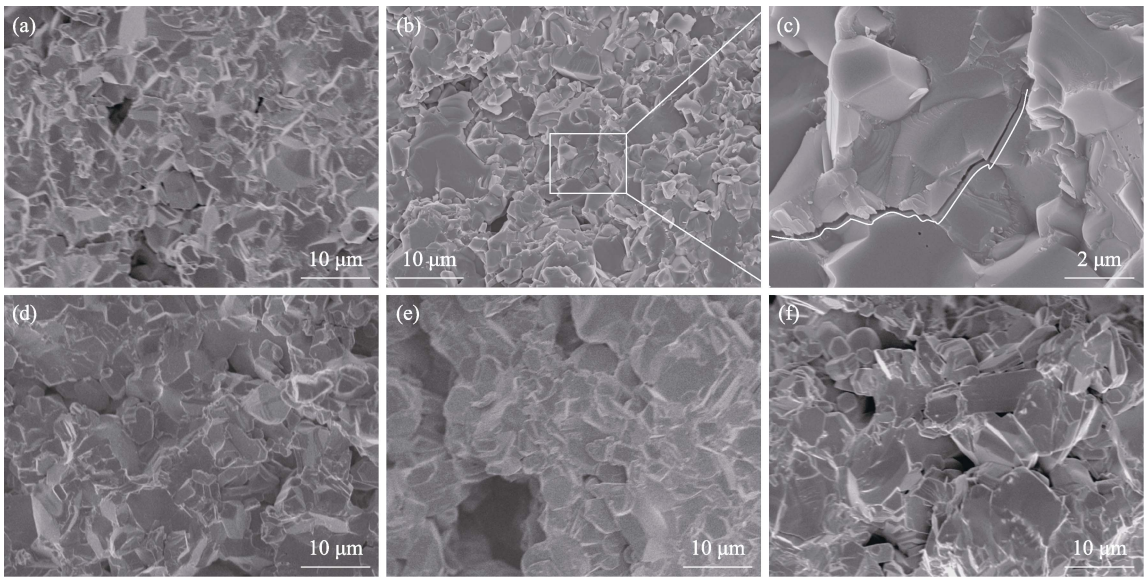


Fig. 5 Fracture microstructures of sintered $Al_2O_3$ ceramics
(a) A45; (b) A50; (c, d) A55; (e) A60; (f) A65

poor strength. The fracture microstructure of sintered $Al_2O_3$ ceramics are given in Fig. 5. After SL, the organics must be removed. Pores are observed in the sintered ceramics due to the volatilization of organics. The degree of densification is mainly related to the particles packing degree, and the solid loading of the initial slurry. Usually, the more the particles packing and the solid loading are, the higher the density is. At a low solid loading of 45% (in volume), correspondingly, the fraction of photosensitive resin is higher, distance between $Al_2O_3$ particles is too far. Thus, some pores were formed in A45 ceramics and density is low (Fig. 5(a)). As the solid loading increasing, pores decreases and density increases (Fig. 5(b)). Moreover, intergranular fracture behavior is found in A50 ceramic (Fig. 5(c)), that is another reason why A50 ceramic has a highest strength. However, when the solid loading is higher than 50% (in volume), the significant increasing of viscosity leads to rise probability of pores and agglomeration during the inhomogeneous recoating process, thus forming pores and other defects in sintered ceramics after debinding and sintering process (Fig. 5(d–f)). The formed defects always cause cracks, thus reducing the strength of $Al_2O_3$ ceramics.

## 3 Discussion

To further investigate the relationship between the UV-light intensity, exposure time and curing thickness, the Jacobs equation derived from the Beer's law[23] can be described:

$$C_p = D_p\left(\ln\frac{E_i}{E_c}\right) \tag{3}$$

where $C_p$ refers to the absolute curing thickness (μm), $D_p$ refers to depth of penetration (μm), $E_i$ and $E_c$ refer to the density of energy transmitted to the slurry (or input density of energy) and critical density of energy ($mJ\cdot cm^{-2}$), respectively. Curing thickness *vs* logarithm of input density of energy curves are shown in Fig. 6(a). The

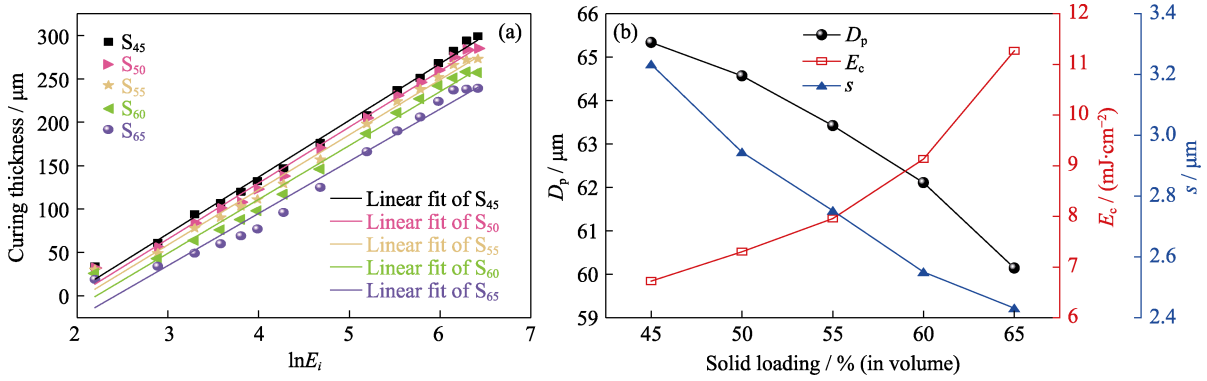


Fig. 6 (a) Curing thickness *vs* logarithm of input density of energy, (b) depth of penetration, critical density of energy and interparticle spacing *vs* solid loading for $Al_2O_3$ slurries

experimental values are in good agreement with the Beer-Lambert's semi-logarithmic model result ($R^2$>0.97). Thus, $D_p$ and $E_c$ of photosensitive $Al_2O_3$ slurries with various solid loadings can be calculated from Fig. 6(a), as plotted in Fig. 6(b). With the solid loading increasing from 45% to 65% (in volume), $D_p$ sharply decreases to 60.14 μm. On the contrary, $E_c$ increases to 11.27 mJ·cm$^{-2}$. These results confirm the findings of Abouliatim[24], who found that apart from particle size, $D_p$ was strong dependent on the solid loading of slurry and decreased with the increasing of solid loading. This can be attributed to the decreasing of the UV-light absorbed by photosensitive resin. On the other hand, high particle packing leads to the decrease of the interparticle spacing between particles, and the path of UV-light increases due to the light refraction of $Al_2O_3$ particles, which causes light loss. An equation introduced by Griffith and Halloran[25] is adopted to describe $D_p$ and the inter-particle spacing ($s$):

$$D_p = \frac{2d_{50}\lambda}{3s\phi}(n_p - n_r)^2 \quad (4)$$

where $d_{50}$ is the average particle size, $\lambda$ refers to the wavelength of radiation, $\phi$ refers to the solid loading of slurry, $n_p$ and $n_r$ refer to the refractive index of $Al_2O_3$ particle and photosensitive resin, respectively. It can be seen from Fig. 6, $s$ correspondingly decreases to 2.43 μm with the increasing of solid loading from 45% to 65% (in volume). The shorter the $s$ between $Al_2O_3$ particles in the slurry is, the greater the probability of mutual contact is, which hinders the movement of the slurry between layers and forms agglomerations.

Although the microstructure of $Al_2O_3$ sintered ceramics has been performed by SEM, and defects have been found, three-dimensional (3D) characterization of structures and defects within the sintered ceramics still needs inspection and discussion. X-CT is one of the most practical ways of non-invasive imaging technology, which can simultaneously carry out both the geometrical features and defects distribution of manufactured parts[26-27]. Fig. 7 presents the X-CT reconstructed images of $Al_2O_3$ sintered ceramics prepared from various slurries. Colored layers in Fig. 7 show internal defects, such as delamination or cracks. And colored points present detected pores, according to their volume. Both delamination defects and pores are detected in all sintered $Al_2O_3$ ceramics. One important finding is that the external area in contact with air shows low defect distribution, rather than internal area. Inevitable pores formed due to the volatilization of the organics as mentioned above within the green body during debinding and sintering process, so the defects near the internal area are difficult to eliminate than those in external areas. The defects

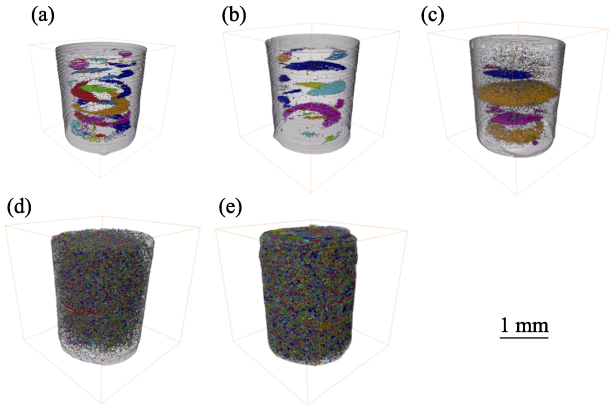


Fig. 7 X-CT reconstructed images of sintered $Al_2O_3$ ceramics (a) A45; (b) A50; (c) A55; (d) A60; (e) A65

decrease firstly and then increase with the increasing of solid loading, which is consistent with the result of relative density. Thus, these manufactured defects that are already critical for the mechanical behavior of sintered $Al_2O_3$ ceramics. Moreover, at the high solid loading of 60% and 65% (in volume) (as shown in Fig. 7(d, e)), it can be obviously found that larger amounts of pores are formed in A60 and A65 sintered ceramics, mainly because the high viscosity leads to rising probability of pores and agglomeration during the inhomogeneous recoating process. These preliminary findings of defects should however be verified by a more extensive quantitative analysis. How to achieve the quantitative analysis of the defects was not the main focus of this paper, and would be investigated in our other study.

It should be noted that although the cylinder green bodies were prepared from photosensitive slurry with different solid loadings, the designed dimensions were same (as shown in Fig. 1(b)). From Fig. 7, it is clearly shown that cylinders present a different shrinkage behavior after debinding and sintering. These results were confirmed by the shrinkage findings, which were measured from the rectangular bars, as shown in Fig. 8. As expected, all different bars prepared from different

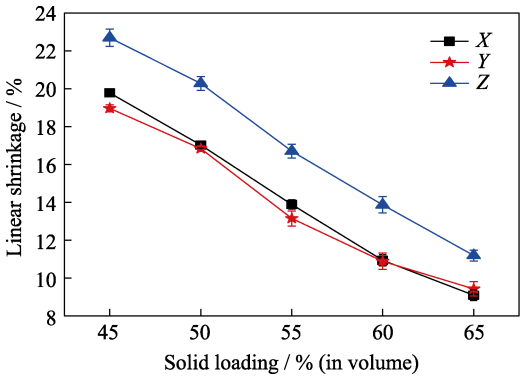


Fig. 8 Linear shrinkage of the rectangular $Al_2O_3$ sintered ceramics in different directions

slurries show significant shrinkage behavior. Out of expectation, different shrinkage values present not only in bars with various solid loadings, but also in different directions. Bars show a similar shrinkage in *X* and *Y* directions, however, a larger shrinkage in *Z* direction is presented because of green bars are manufactured by SL additive manufacturing based layer-by-layer recoating of ceramic slurry along building direction, the interlayers binding in building direction (*Z* direction) is slightly weaker than the cured photosensitive slurry in *X* and *Y* directions. These objects can be eliminated after debinding and sintering process, thereby presenting a larger shrinkage[10-11,28]. This anisotropic shrinkage in different directions corresponds to the accurate prediction and control of the final ceramic product dimensions achieved with SL additive manufacturing.

# 4 Conclusions

In this study, the effect of solid loading on rheological behavior and curing properties of photosensitive $Al_2O_3$ slurry were investigated and discussed deeply. Results showed that both the viscosity and shear stress increased with the increasing of solid loading. The optimal exposure time was selected as 4 s. Then, both the highest relative density of (94.46±0.41)% and flexural strength of (279.54±6.82) MPa are obtained from the photosensitive slurry with a solid loading of 50% (in volume), respectively. A further increase in solid loading has a negative effectiveness on the densification of sintered $Al_2O_3$ ceramics resulting from rise probability of pores and agglomeration during the inhomogeneous recoating process, which provides no improvement of mechanical of $Al_2O_3$ ceramic. Both delamination and pores are detected in SL additive manufactured $Al_2O_3$ ceramics. These manufactured defects that are already critical for the mechanical behavior of $Al_2O_3$ sintered ceramic should be verified by a more extensive quantitative analysis in future study.

## References:


[1] LAKHDAR Y, TUCK C, BINNER J, *et al.* Additive manufacturing of advanced ceramic materials. *Progress in Materials Science*, 2021, **116:** 100736.

[2] LI X B, ZHONG H, ZHANG J X, *et al.* Powder characteristics on the rheological performance of resin-based zirconia suspension for stereolithography. *Journal of Inorganic Materials*, 2020, **35(2):** 231–235.

[3] HE C, MA C, LI X L, *et al.* Continuous fast 3D printing of SiOC ceramic components. *Additive Manufacturing*, 2021, **46:** 102111.

[4] YANG L L, ZENG X J, DITTA A, *et al*. Preliminary 3D printing of large inclined-shaped alumina ceramic parts by direct ink writing. *Journal of Advanced Ceramics*, 2020, **9:** 312–319.

[5] HU X A, ZHAO G L, LIU F C, *et al*. Microstructure and mechanical behavior of Inconel 625 alloy processed by selective laser melting at high temperature up to 1000 ℃. *Rare Metal*, 2020, **39:** 1181–1189.

[6] CHEN F, ZHU H, WU J M, *et al.* Preparation and biological evaluation of $ZrO_2$ all-ceramic teeth by DLP technology. *Ceramics International*, 2020, **46(8):** 11268–11274.

[7] ZHANG K Q, XIE C, WANG G, *et al.* High solid loading, low viscosity photosensitive $Al_2O_3$ slurry for stereolithography based additive manufacturing. *Ceramics International*, 2019, **45(1):** 203–208.

[8] CHEN Z W, LI Z Y, LI J J, *et al*. 3D printing of ceramics: a review. *Journal of the European Ceramic Society*, 2019, **39(4):** 661–687.

[9] HE R J, ZHOU, N P, ZHANG K Q, *et al.* Progress and challenges towards additive manufacturing of SiC ceramic. *Journal of Advanced Ceramics*, 2021, **10(4):** 637–674.

[10] SU B, DHARA S, WANG L. Green ceramic machining: a top-down approach for the rapid fabrication of complex-shaped ceramics. *Journal of the European Ceramic Society*, 2008, **28(11):** 2109–2115.

[11] LI H, LIU Y S, LIU Y S, *et al*. Microstructure and mechanical properties of 3D printed ceramics with different vinyl acetate contents. *Rare Metals*, 2021, **40:** 3241–3250.

[12] DING G J, HE R J, ZHANG K Q, *et al.* Dispersion and stability of SiC ceramic slurry for stereolithography. *Ceramics International*, 2020, **46(4):** 4720–4729.

[13] LI K H, ZHAO Z. The effect of the surfactants on the formulation of UV-curable SLA alumina suspension. *Ceramics International*, 2017, **43(6):** 4761–4767.

[14] NIE J B, LI M S, LIU W W, *et al.* The role of plasticizer in optimizing the rheological behavior of ceramic pastes intended for stereolithography-based additive manufacturing. *Journal of the European Ceramic Society*, 2021, **41(1):** 646–654.

[15] AZARMI F, ALI A. Microstructural evolution during fabrication of alumina *via* laser stereolithography technique. *Ceramics International*, 2019, **45(1):** 271–278.

[16] NDINISA S S, WHITEFIELD D J, SIGALAS I. Fabrication of complex shaped alumina parts by gelcasting on 3D printed moulds. *Ceramics International*, 2020, **46(3):** 3177–3182.

[17] WEI J J, LI J L, SONG X X, *et al.* Effects of solid loading on the rheological behaviors and mechanical properties of injection-molded alumina ceramics. *Journal of Alloys and Compounds*, 2018, **768:** 503–509.

[18] ZHANG K Q, HE R J, DING G J, *et al.* Digital light processing of 3Y-TZP strengthened $ZrO_2$ ceramics. *Material Science Engineering A*, 2020, **774:** 138768.

[19] ISO 14704-2000. Fine Ceramics-Test Method for Flexural Strength of Monolithic Ceramics at Room Temperature.

[20] HERSCHEL W H, BULKLEY R. Konsistenzmessungen von gummi-benzollosungen. *Kolloid Zeitschrift*, 1926, **39:** 291–300.

[21] LEWIS J A. Colloidal processing of ceramics. *Journal of the American Ceramic Society*, 2000, **83:** 2341–2359.

[22] LIU D M. Particle packing and rheological property of highly-concentrated ceramic suspensions: $\varphi_m$ determination and viscosity prediction. *Journal of Materials Science*, 2000, **35(21):** 5503–5507.

[23] CHARITIER T, CHAPUT C, DOREAU F, *et al*. Stereolithography of structural complex ceramic parts. *Journal of Materials Science*, 2002, **37:** 3141–3147.

[24] ABOULIATIM Y, CHARTIER T, ABELARD P, *et al*. Optical characterization of stereolithography alumina suspensions using the Kubelka-Munk model. *Journal of the European Ceramic Society*, 2009, **29(5):** 919–924.

[25] GRIFFITH M L, HALLORAN J W. Freeform fabrication of ceramics *via* stereolithography. *Journal of the American Ceramic Society*, 1996, **79:** 2601–2608.
[26] DIENER S, FRANCHIN G, ACHILLES N, *et al*. X-ray microtomography investigations on the residual pore structure in silicon nitride bars manufactured by Direct Ink Writing using different printing patterns. *Open Ceramic*, 2021, **5:** 100042.
[27] ZHANG K Q, MENG Q Y, CAI N J, *et al*. Effects of solid loading on stereolithographic additive manufactured $ZrO_2$ ceramic: a quantitative defect study by X-ray computed tomography. *Ceramics International*, 2021, **47(17):** 24353–24359.
[28] ZHANG K Q, HE R J, DING G J, *et al*. Effects of fine grains and sintering additives on stereolithography additive manufactured $Al_2O_3$ ceramic. *Ceramics International*, 2021, **47(1):** 2303–2310.

# 立体光刻增材制造中固含量对 $Al_2O_3$ 陶瓷性能的影响

刘国仟[1], 闫长海[1], 张可强[2], 金 华[3], 何汝杰[2]

(1. 中国运载火箭技术研究院 空间物理重点实验室, 北京 100076; 2. 北京理工大学 先进结构技术研究院, 北京 100081; 3. 厦门大学 航空航天学院, 厦门 361005)

**摘 要:** 对于陶瓷立体光刻增材制造技术, 光敏树脂浆料的固含量发挥着重要的作用。本工作首先制备了不同固含量的 $Al_2O_3$ 陶瓷浆料, 并采用立体光刻增材制造技术, 制备了 $Al_2O_3$ 陶瓷, 并研究了 $Al_2O_3$ 浆料的固含量与陶瓷性能的关联关系。其次, 探索了固含量对 $Al_2O_3$ 浆料的流变行为、固化性能, 以及对 $Al_2O_3$ 陶瓷的微观结构、力学性能的影响规律。结果表明, 随着固含量增加, 浆料的粘度和剪切应力均增大。在光固化增材制造过程中, 高固含量导致浆料的粘度高于其自流平的临界值, 且 $Al_2O_3$ 浆料的固化性能与固含量高度相关。此外, 固含量明显影响光固化增材制造的 $Al_2O_3$ 陶瓷的缺陷。这些制造缺陷对于 $Al_2O_3$ 陶瓷的力学性能有重要影响。最后, 本工作总结了光敏 $Al_2O_3$ 浆料的流变行为、固化性能与 $Al_2O_3$ 陶瓷的微观结构和力学性能之间的关联关系。浆料的高粘度造成陶瓷的微观结构不均匀, 最终导致其力学强度较差。本研究结果可为陶瓷的光固化增材制造提供一定的参考。

**关 键 词:** $Al_2O_3$ 陶瓷; 固含量; 光固化; 增材制造

**中图分类号:** TQ174 **文献标志码:** A